

INTERFEROMETER BEAM SIZE MEASUREMENTS IN SPEAR3 §

J. Corbett, W. Cheng, A.S. Fisher, E. Irish (SLAC), T. Mitsuhashi (KEK) and
W. Mok (Life Imaging Technology)

Abstract

A two-slit interferometer has been installed in the SPEAR3 diagnostic beam line to measure vertical beam size at a dipole source point. The unfocused visible light initially passes through a 3.5x6.0mrad aperture and expands to 100mm vertical height at the interferometer slits 17m from the source. For typical emittance coupling factors $\chi \sim 0.3-0.5\%$, $\sigma_y \sim 20\mu\text{m}$ at the source point and a slit separation of 50mm produces fringe visibility $V=0.7$. Hence, a significant plot of fringe visibility vs. slit separation can be generated to infer source size via Fourier transform. In this paper we report on interferometer construction, beam size measurements, skew quadrupole coupling compensation and local coupling correction for the BL13 EPU.

INTRODUCTION

As new science demands increasingly high-brightness photon beams for x-ray imaging and small cross-section beams for high-energy physics, transverse beam dimensions become progressively more difficult to measure. X-ray pinhole cameras have recently been pushed to state-of-the-art limits [1,2] but may not be able to resolve the few-micron vertical beam sizes anticipated in future light sources. Direct visible/UV light imaging does not have adequate resolution but techniques such as π -mode null-measurement [3], Fresnel zone-plate imaging [4] and the use of URA's [5] are useful in this regime and will likely find future application.

The stellar interferometer, however, first applied by Mitsuhashi to image a storage ring beam [6], is well suited to the modest vertical beam size (10-30 μm rms) and diagnostic beam line configuration at SPEAR3. In this paper, we review the SPEAR3 interferometer configuration and report on vertical beam size measurements under nominal and small x-y coupling conditions and effects introduced by the BL13 EPU.

THE STELLAR INTERFEROMETER

The use of a wavefront-division interferometer to measure electron beam size follows closely the early work of Michelson who developed and applied the technique to measure stellar diameters. Although stars are far in the distance, their statistically 'thermal' radiation carries with it a spatial 'degree of coherence' as would any spherical wavefront emitted by a point source at infinity. In the textbook 2-slit interference experiment using a plane wave, the perfect spatial coherence of the radiation generates 100% sinusoidal modulation or visibility $V=1.0$

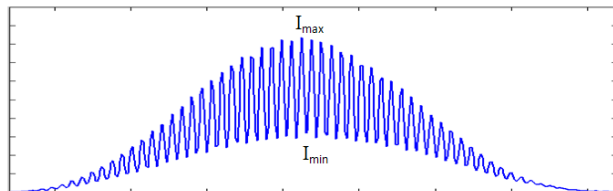


Figure 1: Typical interference pattern at SPEAR3 demonstrating sinc^2 and sinusoidal intensity modulation.

on the image screen. For an incoherent source of finite size, however, wavefronts emitted from each differentially radiating point on the source have a slightly different relative travel time to each slit as compared to other points on the source. As a result, the differential intensity patterns are phase-shifted on the screen resulting in a 'smeared' interference pattern (Figure 1). The source is said to be *partially* coherent and the contrast, or visibility

$$V = (I_{\max} - I_{\min}) / (I_{\max} + I_{\min}) \quad (1)$$

is reduced to a value less than unity. As the slits are further separated, the phase-shift effect is enhanced and the visibility reduced. At the heart of the Van-Cittert/Zernike theorem we find that under sufficiently 'linear' conditions the Fourier transform of the visibility function plotted as a function of slit separation yields the spatial intensity profile of the incoherent source [7]. For Gaussian beams, the result is particularly simple.

THE SPEAR3 INTERFEROMETER

The diagnostic beam line at SPEAR3 accepts visible/UV dipole radiation through a 3.5x6mrad hard aperture. The x-ray core of the beam is shadowed by a 0.6mrad copper beam-block at the midplane and the remaining beam is deflected 18° horizontally by a Rh-coated Si mirror in the accelerator tunnel. After transiting three Quartz windows and a two-bounce mirror configuration at near-normal incidence, the centerline of the beam emerges 15cm above the optical bench.

The two interferometer slits are located in front of a 150mm diameter, $f=2\text{m}$ doublet lens 17m from the source. The slit elevations are manually adjustable on a post outfitted with a vertical gear track. At a distance 1.5m downstream from the doublet, a final near-normal incidence folding mirror directs the two interfering beamlets through a 550nm, 10nm FWHM bandpass filter, a Glan-Thompson polarizer and an $f=150\text{mm}$ lens to image the source onto a 12-bit, 4.65 μm pixel CCD camera [8]. A MATLAB graphical interface controls the camera and displays both the raw image and classical interference pattern to the screen. Typical camera exposure times are 25-50 ms at 100mA beam current.

§Work supported by US Department of Energy Contract DE-AC03-76SF00515 and Office of Basic Energy Sciences, Division of Chemical Sciences.

For sufficiently equal beam intensities at each slit, the measured interference pattern can be fit to

$$I(y) = I_0 + I_1 \sin c^2(A(y - y_1))[1 + V \cos(B(y - y_2))] \quad (2)$$

where $\{I_0, I_1, A$ and $B\}$ are intensity and frequency fitting variables, the sinc^2 term is due to the finite slit openings, V is the visibility and (y_1, y_2) are phase factors. A more complete derivation of the interference pattern including finite bandpass filter effects can be found in [9]. In practice the fitting algorithm first fits sinc^2 to estimate A and y_1 , performs an FFT near y_1 to estimate B, y_2 , and finally fits Equation 1 to yield visibility V .

Due to the low emittance coupling in SPEAR3 ($\chi \sim 0.05\text{-}0.5\%$), the vertical beam size at the dipole source point can range from $8\mu\text{m}$ to $25\mu\text{m}$ ($\beta_y = 14.6\text{m}$, $\epsilon_x = 10\text{nm-rad}$). At 17m from the source, the spatial degree-of-coherence is therefore high, which forces the slit separation to values of 40-80mm in order to yield fringe visibilities in the range $V = 0.4\text{-}0.9$. As a result of the large slit separation, however, the interference pattern has a high spatial-frequency at the camera CCD and the image suffers from quantization effects due to the finite pixel size. Typical sample rates are $\sim 10\text{px/period}$ of the interference pattern.

Since it is essential to detect extreme values of both maxima and minima to determine true visibility, we numerically fit the interference pattern to Eq. (2) above. For small beam sizes, the fitting process can yield a 3-5% increase in visibility relative to a direct read of I_{max} and I_{min} from the sampled waveform, and produce over 10% reduction in calculated beam size. The ultimate resolution of the interferometer is limited by system vibration, wavefront distortion at optical elements and camera linearity, etc [10]. A raw image and section of fitted data near center of the vertical interference pattern are shown in Figure 2.

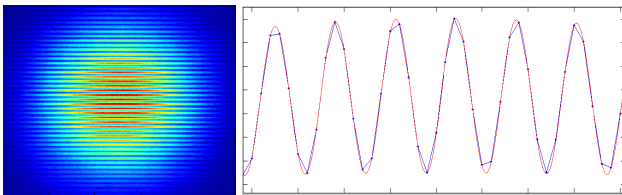


Figure 2: Raw image and vertical lineout with fit.

BASELINE MEASUREMENTS

For a Gaussian beam profile at the source the visibility V is also a Gaussian function of slit separation d with peak value unity:

$$V(d) = \exp\left(-\frac{d^2}{2\sigma_d^2}\right) \quad (3)$$

As discussed above, the Fourier transform yields the intensity profile of the source

$$I(y) = \frac{1}{\sqrt{2\pi}\sigma_y} \exp\left(-\frac{y^2}{2\sigma_y^2}\right) \quad (4)$$

where

$$\sigma_y = \frac{\lambda L}{2\pi\sigma_d} \quad (5)$$

is the rms vertical beam size. By solving for σ_d from Eq. 5 and substituting into Eq. 3 the expression for beam size as a function of fringe visibility for fixed separation d is

$$\sigma_y = \frac{\lambda L}{\pi d} \sqrt{\frac{1}{2} \ln\left(\frac{1}{V}\right)} \quad (6)$$

A plot of fringe visibility measured as a function of interferometer slit separation for the case of nominal electron beam optics and nominal coupling ratio is shown in Figure 3. For this case we fit the data ± 150 points on each side of center in the interference pattern to yield $V(d)$ and set $V=1.0$ at $d=0.0\text{mm}$. The Gaussian fit superimposed on the visibility data points indicates an rms value of $\sigma_d = 64\text{mm}$. From Eq. 5, the corresponding vertical beam size is $\sigma_y = 23.2\mu\text{m}$ ($\lambda = 550\mu\text{m}$, $L = 17\text{m}$). If we apply a system resolution of $10\mu\text{m}$, then by de-convolution the vertical beam size is

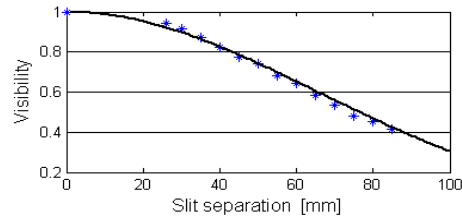


Figure 3: Visibility vs. slit separation with $\sigma_d = 64\text{mm}$.

$\sigma_y = \sqrt{23.2^2 - 10^2} = 21\mu\text{m}$. Under the assumption of zero vertical dispersion at the source, the emittance coupling ratio is $\chi \sim 0.3\%$.

COUPLING CORRECTION

SPEAR3 presently operates with a coupling factor $\chi \sim 0.3\%$ to yield a beam lifetime of 40hr at 100ma. Coupling correction is made with a set of 15 skew quadrupole windings mounted on discrete sextupole magnets. To test the response of the interferometer to changes in vertical beam size, the entire set of skew quads was varied in unison to vary the x-y coupling.

By applying weighting factors to minimize the vertical dispersion, LOCO analysis can generate coupling factors of order $\chi < 0.1\%$. To optimize waveform sampling on the CCD, the interferometer slit separation was fixed at $d = 50\text{mm}$ for the coupling measurement and the vertical beam size computed from Equation 6. As noted in [10], the separation of the interferometer slits should be set to give a visibility of $V = 0.6$ for minimum sensitivity to measurement error.

The skew quad pattern was then adjusted to produce the variation in interferometer visibility shown in Figure 4a (left). Since the slit separation was only $d = 50\text{mm}$, the visibility reached a high, non-optimum value of $V > 0.9$ leading to some uncertainty in the measurement. The beam size data shown in Figure 4b (right) was again processed using a $10\mu\text{m}$ de-convolution factor to account for overall system resolution. At minimum coupling the vertical beam size is under $10\mu\text{m}$.

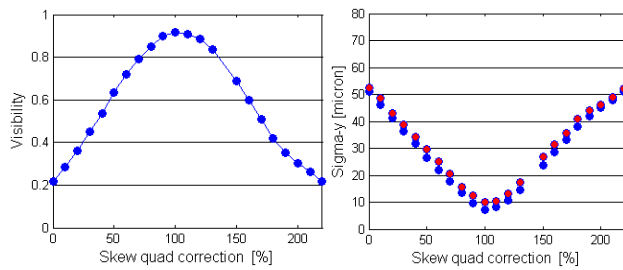


Figure 4: Visibility and vertical beam size variation as measured with interferometer (blue) and pinhole camera (red) as a function of skew-quad correction.

Simultaneous x-ray pinhole measurements are also plotted in Figure 4b (red). For the pinhole data a $15\mu\text{m}$ de-convolution factor was used to reach the final result. Functionally the agreement between the pinhole and the interferometer data is quite good.

A straightforward calculation of the coupling factor

$$\chi = \frac{\sigma_y^2}{\epsilon_x \beta_y} \quad (7)$$

from the interferometer data yields the plot shown in Figure 5. When the skew quadrupole correction is removed, the ‘bare’ lattice coupling factor with insertion devices active is $\sim 1.5\%$. With full skew quadrupole correction the coupling factor reaches $\chi \sim 0.06\%$.

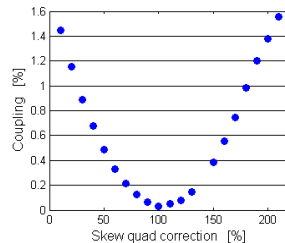


Figure 5: x-y emittance coupling.

EPU COUPLING MEASUREMENTS

One of the more difficult effects to correct in a storage ring can be the skew quadrupole field from an elliptically-polarizing undulator (EPU). To compensate for the skew-induced coupling caused by gap changes in the SSRL EPU [11], a feed-forward table drives a local skew quadrupole coil.

To further investigate the impact of the EPU, the interferometer was again operated in the fixed slit-separation mode ($d=50\text{mm}$) with the nominal coupling corrector pattern to monitor vertical beam size (Eq. 5). Figure 6 shows the impact of the un-compensated EPU (left) and the effect of the skew coil with the EPU at 20mm minimum gap (right). In terms of coupling, the EPU fields will increase χ from 0.3% to 0.9% if left un-compensated in the current storage ring optics. As shown in Figure 7, however, the skew-quad feed-forward table developed with LOCO reduces the EPU coupling effect to negligible values.

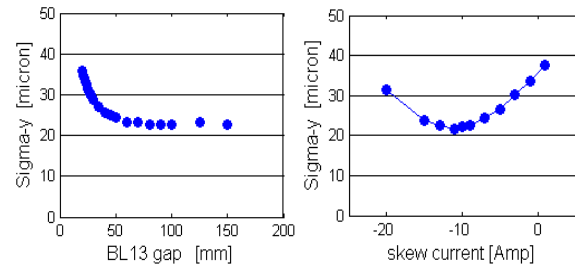


Figure 6: Vertical beam size as a function of un-compensated EPU gap (left) and as a function of skew coil with 20mm EPU gap (right).

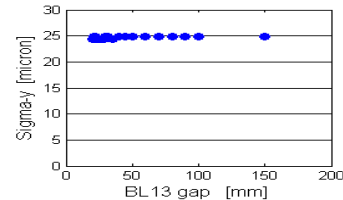


Figure 7: Plot of vertical beam size demonstrating EPU coupling compensation by skew quad feed-forward tables.

ACKNOWLEDGEMENTS

The authors would like to thank T. Mitsuhashi for sharing the fine art of slit production and nuances of interferometer theory, J. Trehwella of the Australian Synchrotron for assistance in data acquisition, and X. Huang and J. Safranek for LOCO operation.

REFERENCES

- [1] C. A. Thomas, G. Rehm, ‘Pinhole Camera Resolution & Emittance Measurement’, EPAC08, Genoa, Italy, 2008.
- [2] M.-A. Tordeux, *et al*, ‘Ultimate Resolution of SOLEIL X-Ray Pinhole Camera’, DIPAC07, Venice, Italy, 2007.
- [3] A. Anderson, ‘Recent Results from the Electron Beam Profile Monitor at the Swiss Light Source’, DIPAC07, Venice, Italy, 2007
- [4] K. Iida, *et al*, ‘Measurement of an Electron-Beam Size with a Beam Profile Monitor using Fresnel Zone Plates’, NIM A506, 2003.
- [5] J. Flanagan, *et al*, ‘X-Ray Monitor Based on Coded-Aperture Imaging for KEK-B Upgrade and ILC Damping Ring’, submitted to PRST-AB.
- [6] T. Mitsuhashi, ‘Beam Profile and Size Measurement by SR Interferometer’ in *Beam Measurements*, Ed. By S. Kurokawa, *et al*, p. 399-427, World Scientific (1999).
- [7] F. Zernike, ‘The Concept of Degree of Coherence and Application to Optical Problems’, *Physica*, Vol. 5, 1938.
- [8] Point Grey Research, Flea Camera www.ptgrey.com
- [9] A. Fisher, ‘Fringe Pattern of the PEP-II Synchrotron-Light Interferometers’, SLAC-TN-05-048, May, 2005.
- [10] T. Mitsuhashi, ‘Twelve Years of SR Monitor Development at KEK’, BIW 2004, Knoxville, Tennessee.
- [11] R. Carr, *et al*, ‘An Elliptically-Polarizing Undulator with Phase Adjustable Energy and Polarization’, SLAC-PUB-6627, October, 1995.